

Superconductivity in SnO: a Nonmagnetic Analog to Fe-based Superconductors?

M. K. Forthaus^{1,†}, K. Sengupta^{1,†}, O. Heyer¹, N. E. Christensen², A. Svane²,

K. Syassen³, D. I. Khomskii¹, T. Lorenz¹, and M. M. Abd-Elmeguid¹

¹*II. Physikalisches Institut, Universität zu Köln, Zùlpicher Str. 77, D-50937 Köln, Germany*

²*Department of Physics and Astronomy, Aarhus University,*

Bygning 1520, Ny Munkegade 120, DK-8000 Aarhus, Denmark and

³*Max-Planck-Institut für Festkörperforschung, Heisenbergstraße 1, D-70569 Stuttgart, Germany*

We found that under pressure SnO with α -PbO structure, the same structure as in many Fe-based superconductors, e.g. β -FeSe, undergoes a transition to a superconducting state for $p \gtrsim 6$ GPa with a maximum T_c of 1.4 K at $p = 9.3$ GPa. The pressure dependence of T_c reveals a dome-like shape and superconductivity disappears for $p \gtrsim 16$ GPa. It is further shown from band structure calculations that SnO under pressure exhibits a Fermi surface topology similar to that reported for some Fe-based superconductors and that the nesting between the hole and electron pockets correlates with the change of T_c as a function of pressure.

PACS numbers: 74.70.Ad, 74.62.Fj, 74.25.Dw, 74.20.Pq

The discovery of superconductivity in the iron-based layered compound $\text{La}(\text{O}_{1-x}\text{F}_x)\text{FeAs}_2$ has led to an explosion of interest not only in experimental and theoretical studies but also in the search for new compounds belonging to the same family of materials. Several other groups of Fe-based superconductors have been found, e.g. $A\text{Fe}_2\text{As}_2$ ($A = \text{Ba}, \text{K}$)³ and more recently β -FeSe^{4,5}. Their common features are layers formed by FeAs tetrahedra, the presence of electron and hole pockets in k -space at the Fermi energy, E_F , and the proximity to a magnetic state. Although the pairing mechanism is still a matter of debate^{6,7}, it is generally believed that superconductivity in FeAs compounds is unconventional with electron pairing possibly mediated by spin fluctuations^{8,9} or a direct electron-hole pair hopping⁷. Among the different types of Fe-based superconductors, the nonmagnetic binary compound β -FeSe ($T_C = 8$ K) is of particular interest owing to its simple structure. β -FeSe has a tetragonal anti- α -PbO type structure ($P4/nmm$) composed of stacked FeSe layers along the c -axis. It is, thus, natural to ask whether compounds with the simple α -PbO structure but which do not contain a transition metal (Fe) would exhibit superconductivity. SnO with the α -PbO-type structure is such a candidate, being a diamagnetic semiconductor at ambient pressure (p) with an electronic structure resembling that of Fe-based systems^{10,11}. Moreover, according to recent infrared and x-ray diffraction measurements SnO becomes metallic at room temperature above $p = 5$ GPa without a change of the lattice structure up to $p \sim 17$ GPa¹². This finding of a pressure-induced metallic state of SnO above ~ 5 GPa is in good agreement with theoretical band structure studies using LDA calculations¹³.

In this work, we show that SnO becomes superconducting under pressure $p \gtrsim 6$ GPa with a maximum T_c of 1.4 K at $p \sim 9$ GPa and that $T_c(p)$ reveals a dome-like shape similar to other Fe-based superconductors. Our band structure calculations indicate that SnO exhibits a Fermi surface topology similar to that reported for Fe-based superconductors and that the nesting between the

hole and electron pockets correlates with $T_c(p)$.

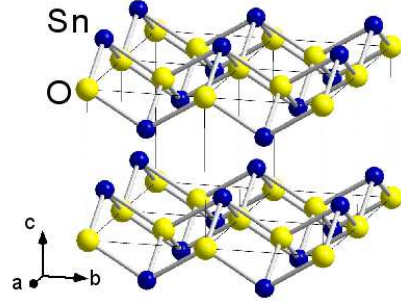


FIG. 1. (color online.) Crystal structure of SnO (α -PbO-type structure ($P4/nmm$)).

For the four-probe electrical resistivity measurement polycrystalline single-phase samples with a stated purity of 99.9% purchased from Alfa Aesar were gently ground and inserted into the sample chamber of a diamond anvil cell (DAC) with a cell body made of a special Ti-alloy to minimize temperature-induced variations of the pressure. Hardened Inconel 750 was used as gasket material, electrical insulation of the gasket from the four gold leads and the sample was provided by a mixture of epoxy and fine Al_2O_3 powder. Pressure was determined at room temperature using the ruby fluorescence method¹⁴. The temperature dependence of the electrical resistivity $\rho(T, p)$ was measured in a ^4He bath cryostat which covers the temperature range $1.6 \text{ K} \leq T \leq 300 \text{ K}$. Measurements at low temperatures ($0.4 \text{ K} \lesssim T \leq 15 \text{ K}$) and in external magnetic fields were performed in a HelioxVL ^3He refrigerator (Oxford Instruments).

Fig. 2(a) displays the temperature dependence of the electrical resistivity $\rho(T)$ in the temperature range $0.4 \text{ K} \leq T \leq 300 \text{ K}$ at selected pressures up to 7.9 GPa using a diamond anvil cell. We find that with increasing pressure the resistivity gradually changes from the

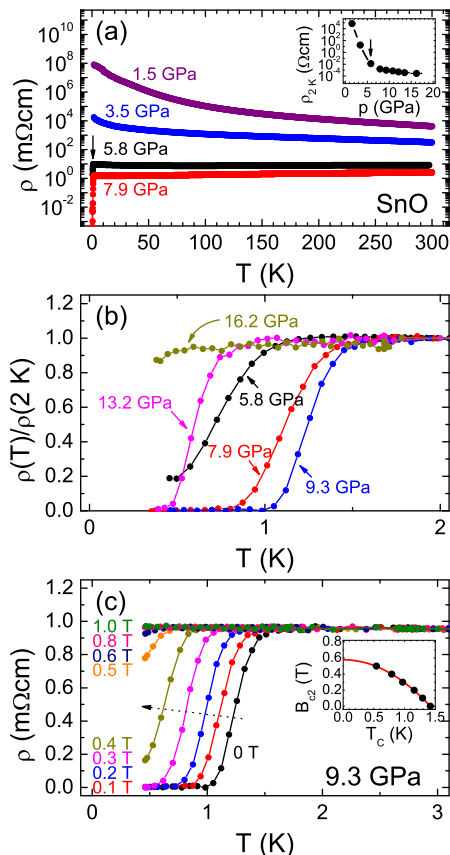


FIG. 2. (color online). (a) Electrical resistivity $\rho(T, p)$ (logarithmic scale) of SnO for $0.4 \text{ K} \lesssim T \leq 300 \text{ K}$ and at different pressures up to 7.9 GPa. The arrow indicates the onset of the superconducting transition for $p \geq 5.8 \text{ GPa}$. The inset shows the pressure dependence of the resistivity at 2 K ($\rho_{2\text{K}}(p)$). The arrow at 5.8 GPa marks the first observation of T_c . (b) Low temperature region ($T \leq 2 \text{ K}$) of $\rho(T)/\rho(2\text{K})$ for different pressures from 5.8 GPa to 16.2 GPa. (c) Effect of an external magnetic field $0 \text{ T} \leq B_{\text{ex}} \leq 1 \text{ T}$ on $\rho(T)$ for 9.3 GPa and $T \leq 3 \text{ K}$. The inset shows $B_{c2}(T_c)$, the red line corresponds to a fit with $B_{c2}(0) = 0.58 \text{ T}$ (see text).

semiconducting to a metallic-like behavior, followed by a sharp drop of $\rho(T)$ ($\sim 80\%$ at 0.35 K at 5.8 GPa) at a critical temperature $T_{\text{onset}} = 1.3 \text{ K}$, indicative of the onset of a superconducting transition. The temperature of the superconducting transition increases with further increase of the pressure to $T_{\text{onset}} = 1.7 \text{ K}$ at 7.9 GPa where the system exhibits zero resistivity at 0.8 K. The proximity of the observed superconducting transition at 5.8 GPa to a semiconductor to metal in SnO transition is demonstrated in the inset of Fig. 2(a). Here, one observes for $p \leq 5.8 \text{ GPa}$ a dramatic decrease of the value of $\rho(2\text{K})$, i.e. the resistivity in the normal state just above the superconducting transition, by more than 6 orders of magnitudes. This decrease becomes distinctly weaker for $5.8 \text{ GPa} \leq p \leq 16.2 \text{ GPa}$. We note that the observation of a metallic-like behavior at $p = 5.8 \text{ GPa}$ is in a good agreement with that reported from high pressure infrared

spectroscopy¹². The superconducting transition temperature T_c for SnO for $5.8 \text{ GPa} \leq p \leq 16.2 \text{ GPa}$ can be seen in Fig. 2(b). Here, it is shown that the superconducting transitions are relatively sharp up to the highest pressure of $p = 13.2 \text{ GPa}$, although we cannot exclude the presence of some pressure gradients in the sample chamber. At 16.2 GPa, we find an onset of the superconducting transition at $\sim 0.6 \text{ K}$, below which $\rho(T)$ drops by 10% down to $\sim 0.4 \text{ K}$. The values of T_c are determined from the temperature at which $\rho(T)$ is reduced by 10% below T_{onset} , i.e. $\rho(T_c)/\rho(T_{\text{onset}}) = 0.9$. The effect of an external magnetic field B_{ex} on the temperature dependence of the electrical resistivity at $p = 9.3 \text{ GPa}$ which corresponds to the maximum value of $T_c = 1.4 \text{ K}$ is shown in Fig. 2(c). As expected for bulk superconductivity, T_c initially shifts linearly to lower temperatures and remains sharp with increasing B_{ex} and can be described by the Werthamer-Helfand-Hohenberg (WHH) theory for “dirty superconductors”¹⁵. This excludes the existence of weak links and/or minority phase superconductivity in the sample. We obtain for the superconducting state of SnO at $p = 9.3 \text{ GPa}$ a value of the upper critical field $B_{c2}(T = 0)$ of about 0.58 T (see inset of Fig. 2(c)) which corresponds to a coherence length $\zeta \approx 240 \text{ \AA}$.

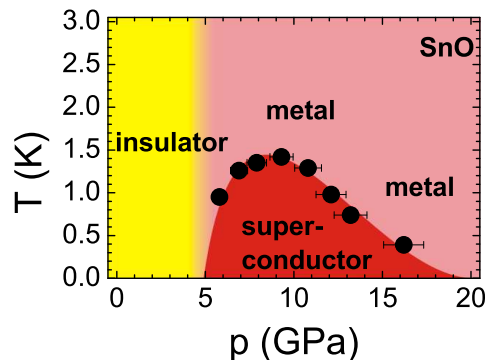


FIG. 3. (color online). Electronic (p, T) phase diagram of SnO. The semiconductor to metal transition is around $\sim 5 \text{ GPa}$. $T_c(p)$ shows a dome-like shape with a maximum ($T_c \sim 1.4 \text{ K}$) around 9 GPa, and decreases gradually for $9 \text{ GPa} \lesssim p \leq 16.2 \text{ GPa}$ with $T_c(16.2 \text{ GPa}) \sim 0.4 \text{ K}$

The results of our high pressure investigation of SnO are summarized in a (p, T) phase diagram in Fig. 3. The pressure dependence of T_c displays a dome-like shape with a maximum value of T_c of about 1.4 K around 9 GPa. T_c increases with increasing pressure with an initial rate of $\partial T_c / \partial p \approx 0.28 \text{ K GPa}^{-1}$ between 5.8 GPa and 6.9 GPa, passes through a maximum around 9 GPa, and then decreases towards zero for $p > 16.2 \text{ GPa}$. This behavior of $T_c(p)$ of SnO resembles that recently reported from high pressure studies on $\beta\text{-FeSe}$ superconducting samples^{16,17}. However, in $\beta\text{-FeSe}$ the value of T_c at ambient pressure is already much higher than the maximum T_c in SnO under high pressure. Also the initial increase of T_c with pressure is stronger for FeSe than we find for SnO in the superconducting phase. On the other hand, in both

cases the initial increase of T_c with pressure is associated with a corresponding decrease of the interlayer distance (Se-Se/Sn-Sn) along the c -axis^{12,16}.

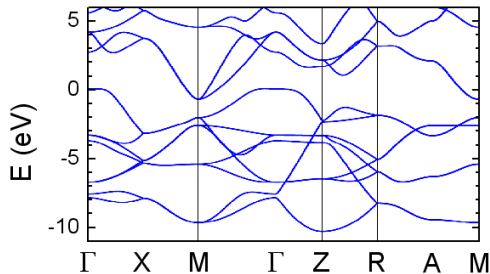


FIG. 4. (color online). The band structure of SnO at 7 GPa. The calculations base on the structural parameters determined by x-ray diffraction experiments¹². The Fermi level is at $E = 0$.

It is interesting to compare the properties of SnO under high pressure with those of Fe-based superconductors. We recall the main ingredients for the occurrence of superconductivity in the latter systems: (i) the existence of several pockets in the Fermi surface with some specific topology; (ii) some degree of nesting is required between the hole and electron pockets; (iii) spin fluctuations associated with such nesting seem to be important. However, the relative importance of the above mentioned ingredients for superconductivity is still a matter of debate. Here, we mention the two most discussed but quite different scenarios. According to Mazin *et al.*⁸ and Kuroki *et al.*⁹, all three factors (i)–(iii) are essential. In this approach superconductivity is induced by the nesting-related antiferromagnetic spin fluctuations near the wave vectors connecting the electron and hole pockets. This leads to an extended s -wave pairing with a sign reversal of the order parameter (s^\pm) between different (nested) Fermi surface sheets. In contrast to this, according to Chubukov⁷, and Kuchinskii and Sadovskii¹⁸ predominantly (i) and (ii) are relevant. These authors proposed, based on a weak coupling approach that spin fluctuations are not necessarily required for an s^\pm state and the pairing mechanism might not be magnetically mediated. It can predominantly originate e.g. from a direct pair hopping between hole and electron Fermi surfaces. We note that here the pockets are important but only nearly nested states are necessary.

In view of the two theoretical approaches mentioned above, it appears that the existence of pockets and some degree of nesting are relevant for the occurrence of superconductivity in Fe-based superconductors. As SnO does not contain magnetic atoms, we explore ingredients (i) and (ii) in the case of SnO. We thus have investigated the Fermi surfaces and nesting properties of metallic SnO and their change with pressure. Fig. 4 illustrates the calculated bands of metallic SnO at 7 GPa along symmetry lines in the Brillouin zone (BZ). These calculations are scalar-relativistic and use the Linear-Muffin-Tin-Orbital

(LMTO) method¹⁹ in a full-potential implementation²⁰. As shown in Fig. 4, the band structure close to E_F is similar to that in FeAs systems^{8,21}: the two bands dipping below E_F near the M-point of the Brillouin zone enclose two electron pockets centered at M whereas the rather flat band slightly above E_F around Γ encloses a hole surface. The states near E_F at M move further down relative to E_F as the pressure is increased, whereas the “hole band” shifts towards higher energies. The indirect band overlap increases with pressure. The “hole band” states as defined here have O- p_z and Sn- s character, whereas the “electron states” close to E_F , around M are of Sn- $p_x p_y$ character (coordinates x , y , and z are along the tetragonal axes, c -axis in the z -direction).

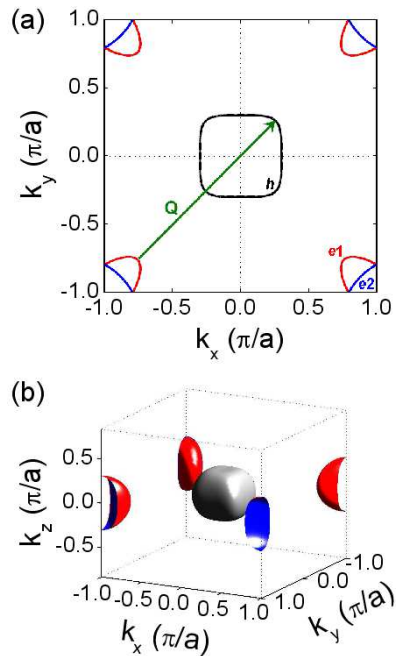


FIG. 5. (color online). (a) Fermi surface contours in the (k_x, k_y) plane as calculated for SnO at 7 GPa. The blue and red curves at the corners (M points) are contours of the electron surfaces, e1 (outer surface, red) and e2 (inner surface, blue). The black curve enclosing the BZ centre (Γ) is the contour of the hole, h, surface. The vector \mathbf{Q} is a representative of nesting vectors in the $(1,1,0)$ directions between the e1 and h surfaces. (b) Fermi surface for SnO calculated at 7 GPa.

Figure 5(a) displays the Fermi surface contours in the (k_x, k_y) plane of the BZ as calculated for SnO at $p = 7$ GPa. We see that the band structure close to E_F and the shape of the Fermi surface of SnO are quite similar to those reported for β -FeSe²¹ and other Fe-based superconductors. The SnO band structure is, however, nearly three-dimensional: the Fermi surface does not exhibit pronounced cylindrical sheets as in FeSe, but has a hole surface of box-like shape (see Fig. 5(b)). However, there is still an efficient nesting between the outer electron surface (e1) and the hole surface (h), see Fig. 5(a). The Fermi surface topology does not change with pres-

sure in the pressure range considered here (5 to 19 GPa), but the degree of nesting between the electron and hole FS changes.

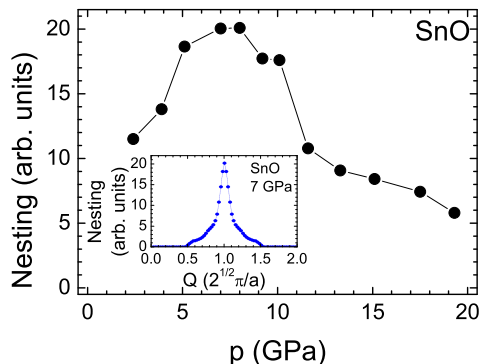


FIG. 6. (color online.) The maximum value of the nesting functions vs. pressure. The values of pressure, volumes, and structural parameters are taken from the experimental values from Ref. 11. The inset shows an example of the calculation of such a nesting function $N(\mathbf{Q})$ for $p = 7$ GPa (see text).

The variation of nesting with pressure illustrated in Fig. 6 has been calculated from the maximum values of the nesting functions for the structural parameters at different pressure points¹². An example of the calculation of such a nesting function $N(\mathbf{Q})$, which is given by $N(\mathbf{Q}) = \int_{\text{BZ}} d^3k \delta(E_{\mathbf{k}} - E_{\mathbf{k}+\mathbf{Q}}) \delta(E_{\mathbf{k}} - E_{\text{F}})$ is shown in the inset of Fig. 6. As evident from Fig. 6, the degree of nesting first increases with increasing pressure, reaches a maximum between 8 and 10 GPa and decreases with further increasing pressure. This behavior correlates with the observed pressure variation of T_c (see (p, T) -phase diagram; Fig. 3). In contrast to this, the calculated density of states at E_{F} , $D(E_{\text{F}})$, as a function of pressure

reveals no remarkable change up to about 20 GPa: while T_c strongly decreases by more than a factor of 3 between 9 GPa and 16 GPa, $D(E_{\text{F}})$ shows only a slight decrease of about 10% in the same pressure range. These theoretical calculations demonstrate that even in the absence of spin fluctuations the Fermi surface topology and nesting properties are relevant to the observed pressure-induced superconductivity in SnO. In such a case the observed superconductivity in metallic SnO with much lower T_c than that found in Fe-based superconductors may be explained in the weak coupling scenario by direct pair hopping between electron and hole pockets⁷. In contrast, spin fluctuations usually lead to strong electronic correlations, i.e. strong coupling and, thereby, higher values of T_c .

In summary, we discovered that SnO, with the α -PbO-type structure, undergoes an insulator-metal transition under pressure at $p_c \sim 6$ GPa and becomes superconducting with $T_c \sim 0.4$ K. With increasing pressure, T_c initially increases up to a maximum of 1.4 K at 9.3 GPa, but then decreases and superconductivity disappears at $p \sim 16$ GPa. The electronic structure of SnO is that of a semi-metal with the hole pocket at the Γ -point and electronic pockets at M-points of the Brillouin zone. Thus, both the crystal and electronic structures of SnO are similar to those of Fe-based superconductors like FeSe or FeAs-systems, but in contrast to these SnO is non-magnetic, and the values of T_c and B_{c2} ($B_{c2} \sim 0.6$ T at 9.3 GPa) are much smaller. We believe that, besides its own interest, the discovery of superconductivity in SnO, the nonmagnetic counterpart of Fe-based superconductors, may be useful for a better understanding of the relative importance of different factors relevant for superconductivity in this class of materials.

This work was supported by the Deutsche Forschungsgemeinschaft (DFG) through SFB 608. K.S. and M.M.A. would like to thank the Alexander von Humboldt foundation for the financial support.

[†] present address: Centro Brasileiro de Pesquisas Físicas, Rio de Janeiro 22290-180, RJ, Brazil
² Y. Kamihara et al., J. Am. Chem. Soc. **130**, 3296 (2008).
³ M. Rotter, M. Tegel, and D. Johrendt, Phys. Rev. Lett. **101**, 107006 (2008).
⁴ F.-C. Hsu et al., Proc. Natl. Acad. Sci. U.S.A. **105**, 14262 (2008).
⁵ T. M. McQueen et al., Phys. Rev. B **79**, 014522 (2009).
⁶ I. I. Mazin and J. Schmalian, Physica C **469**, 614 (2009).
⁷ A. V. Chubukov, Physica C **469**, 640 (2009).
⁸ I. I. Mazin et al., Phys. Rev. Lett. **101**, 057003 (2008).
⁹ K. Kuroki et al., Phys. Rev. B **79**, 224511 (2009).
¹⁰ I. Lefebvre et al., Phys. Rev. B **58**, 1896 (1998).
¹¹ G. W. Watson, S. C. Parker, and G. Kresse, Phys. Rev. B **59**, 8481 (1999).
¹² X. Wang et al., Phys. Status Solidi B **241**, 3168 (2004).

¹³ N. E. Christensen, A. Svane, and E. L. Peltzer y Blancá, Phys. Rev. B **72**, 014109 (2005).
¹⁴ K. Syassen, High Pressure Res. **28**, 75 (2008), and references therein.
¹⁵ N. R. Werthamer, E. Helfand, and P. C. Hohenberg, Phys. Rev. **147**, 295 (1966).
¹⁶ S. Medvedev et al., Nature Mater. **8**, 630 (2009).
¹⁷ D. Braithwaite et al., J. Phys.: Condens. Matter **21**, 232202 (2009).
¹⁸ E. Z. Kuchinskii and M. V. Sadovskii, JETP Lett. **89**, 156 (2009).
¹⁹ O. K. Andersen, Phys. Rev. B **12**, 3060 (1975).
²⁰ M. Methfessel, M. van Schilfgaarde, and R. A. Casali, *Lecture Notes in Physics*, volume 535, Springer-Verlag, Berlin, 2000.
²¹ A. Subedi et al., Phys. Rev. B **78**, 134514 (2008).